Supporting information

Electrocatalytic Strategy for Biomass Upgrading: Highly Selective Conversion of Glycerol to Formic Acid via $NiMoO_4$@CuO/CF Catalysis

Gang Yan,[1*] Jiyao Zhang,[1] Huaqiao Tan[2]*

College of Material Science and Engineering, Jilin Jianzhu University, Changchun 130118, China[1]

Key Laboratory of Polyoxometalate and Reticular Material Chemistry of Ministry of Education, Faculty of Chemistry, Northeast Normal University, Changchun, Jilin 130024, China[2]

Corresponding author:yang431@nenu.edu.cn tanhq870@nenu.edu.cn;

1. Experimental Section

1.1 Chemical and Reagents.

Copper foam (CF, thickness: 4 mm) was purchased from Changsha Lyrun Material Co., Ltd. Copper foam first was cleaned with diluted HCl, acetone, and deionized water for three times to remove surface oil and oxide layers. Then the cleaned CF is cut into a rectangle of 4*0.5 cm. Nickel sulfate hexahydrate $NiSO_4 \cdot 6H_2O$, Ammonium molybdate tetrahydrate $(NH_4)_6Mo_7O_{24} \cdot 4H_2O$, Sodium hydroxide NaOH, Ammonium persulfate $(NH_4)_2S_2O_8$, Ammonia solution $NH_3 \cdot H_2O$, were purchased from Shanghai Aladdin Bio-Chem Technology Co.,LTD. Highly purified water (> 18 MΩ*cm resistivity) was provided by a PALL PURELAB Plus system.

1.2 Synthesis of $Cu(OH)_2$nanowires grown on copper foam.

$Cu(OH)_2$ nanowires arrays were grown on copper foam by simple hydrothermal method. Briefly, 0.7 g $(NH_4)_2S_2O_8$and 2 g NaOH were dissolved in 25 mL distilled water. After stirring for 30 min, this solution was transferred to PTFE stainless steel autoclave. The cleaned CF foam with size about 4*0.5 cm was vertically placed in the autoclave. $Cu(OH)_2$ nanowires were obtained after heated the solution at 40 ℃ for 30min. After cooled down to room temperature, the as-prepared sample was cleaned with distilled water and further dried at 60℃ for 1h.

1.3 Synthesis of CuO nanowires grown on copper foam.

For the preparation of CuO/CF, the $Cu(OH)_2$/CF precursor was calcined in a muffle furnace under air. The temperature was ramped to 300 °C at 5 °C $min^{-1,}$ maintained for 2 h, and the sample was allowed to cool to room temperature; the product was named CuO /CF.

1.4 Synthesis of $NiMoO_4$@CuO nanosheets arrays.

For the preparation of $NiMoO_4$@CuO/CF, 0.394 g of $NiSO_4 \cdot 6H_2O$ and 1.85 g of $(NH_4)_6Mo_7O_{24} \cdot 4H_2O$ were dissolved in 40 mL of deionized water. The resulting solution was transferred into a 50 mL Teflon-lined stainless-steel autoclave, and a piece of CuO/CF was positioned inside the liner with its surface inclined at approximately 60° to the inner wall. The autoclave was sealed and kept at 100 °C for 5 h. Upon completion of the hydrothermal treatment, the sample was rinsed thoroughly with deionized water and dried in an oven at 60 °C, the product named $NiMoO_4$@CuO/CF.

1.5 In-situ Raman spectroscopy.

For in-situ Raman measurements, a confocal Raman spectrometer (InViaQontor) with a 532 nm excitation laser was used. Potentials were controlled by a CHI 660E electrochemical workstation (Shanghai CHENHUA Instrument Co., Ltd.). The in-situ electrochemical Raman experiments were performed in an H-type Raman cell separated by a Nafion proton-exchange membrane (DuPont Nafion 117). $NiMoO_4$@CuO/CF was placed flat at the bottom of the Raman cell so that the sample surface was perpendicular to the incident laser. A carbon rod and an Hg/HgO (1 M KOH) reference electrode were used as the counter and reference electrodes, respectively. The electrolyte was a mixed solution of 1 M KOH and 0.1 M glycerol.

1.6 Electrochemical measurement

Electrochemical measurements were carried out in a conventional three electrode configuration using a CHI660D workstation in an H-type cell. The two compartments were separated by a Nafion 117 membrane (DuPont) pretreated according to reported procedures. Catalyst coated electrodes were used as the working electrode, an Hg/HgO (1 M KOH) reference electrode served as the reference, and carbon rod was used as the counter electrode. The electrolyte was Ar-saturated 1 M KOH (pH = 14) containing 0.1 M glycerol. All potentials were converted to the RHE scale using $E_{RHE}=E_{HgO/Hg}+0.098+0.0591\times pH$. Current densities were normalized to the geometric electrode area (~2.0 cm^2); the electrode area for measurements in 0.1 M glycerol was 2.0 cm^2. Electrocatalytic activity was evaluated by linear sweep voltammetry (LSV) at 5 mV s^{-1}. Long-term stability of $NiMoO_4$@CuO/CF was examined at −0.20 V vs. RHE by amperometric i–t (current–time) measurements.

1.7 Characterization

The morphology and microstructure of the as-prepared samples were investigated by scanning electron microscope (SEM Zeiss Gemini SEM 500) and Lorenz Transmission Electron Microscope (TEM, Talos F200X). The X-ray diffraction (XRD) patterns of samples were recorded on a Bruker D8 ADVANCE using a Cu Kα radiation (λ=1.5418 Å). The X-ray photoelectron spectroscopy (XPS) spectrums of samples were obtained from a Thermo Scientific EscaLab 250Xi with an Al monochromatic X-ray source (1486.6 eV). All binding energies (BEs) were referenced to the C 1s hydrocarbon peak at 284.8 eV.

1.8 Product Analysis.

The conversion rate of glycerol ($\eta_{glycerol}$) and the product selectivity of C1 product ($S_{C1\ product}$, respectively) can be calculated using the following equations:

$$\eta_{glycerol} = \frac{(C_{0,glycerol} - C_{glycerol})}{C_{0,glycerol}} \times 100\% \qquad (formula\ 1)$$

$$S_{C1\ product} = \frac{C_{C1\ product} \times (1/3)}{C_{0,glycerol} - C_{glycerol}} \times 100\% \qquad (formula\ 2)$$

The Faraday efficiency (FE) of $NiMoO_4$ catalyst for formate is calculated based on the following equation:

$$FE\ (for\ NiMoO4) = \frac{C_{formate} \times (1/3) \times 8}{Q_{total}} \times V \times F \times 100\% \qquad (formula\ 3)$$

Using the experimental values $C_{0\_glycerol}$ = 10.0 mM, $C_{glycerol} \approx 0$ mM, C_{FA} = 25.3 mM, V = 0.0151 L and Q_{passed} = 109 C , application of formula 1 gives glycerol conversion = (10.0 − 0)/10.0 × 100% = 100.0%; application of formula 2 converts formate to equivalent glycerol moles as 25.3 mM × (1/3) = 8.433 mM, and dividing by the consumed glycerol (10.0 mM) yields formate selectivity = 84.33%; application of formula 3 gives $n_{FA} = C_{FA} \times V = 0.0253\ mol \cdot L^{-1} \times 0.0151\ L = 3.8203 \times 10^{-4}$ mol, with the common literature electron count that 1 glycerol → 3 $HCOO^-$ requires 8 e^- (i.e., 8/3 e^- per $HCOO^-$), $Q_{theoretical} = n_{FA} \times (8/3) \times F \approx 3.8203 \times 10^{-4} \times 2.6667 \times 96485\ C \cdot mol^{-1} \approx$ 98.29 C, and therefore FE_{FA} = 98.29 / 109 × 100% ≈ 90.2%.

2.Supporting Figures

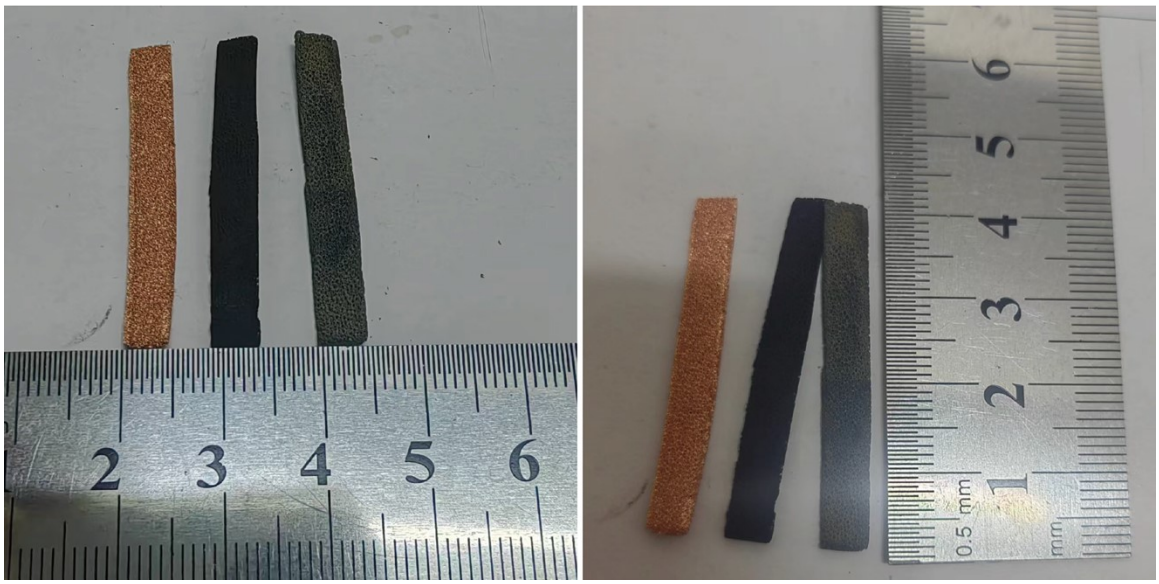

Fig. S1. From left to right are the photographic images of the copper foam, CuO/CF nanowire arrays, $NiMoO_4$@CuO/CF nanosheets arrays. These colour changes can further confirm that the corresponding catalysts are grown on the copper foam.

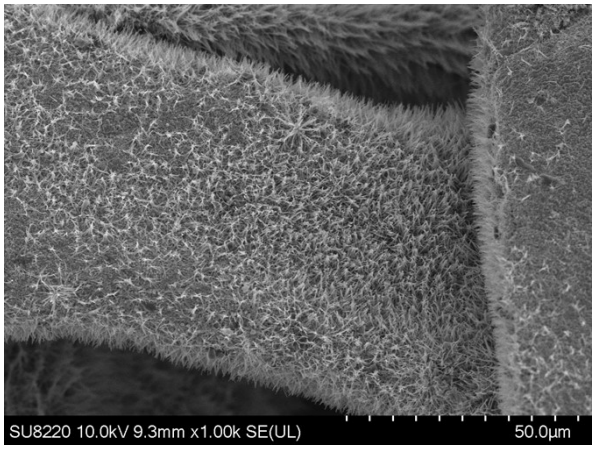

Fig. S2. The morphology of $Cu(OH)_2$/CF nanowires arrays grown on the copper foam.

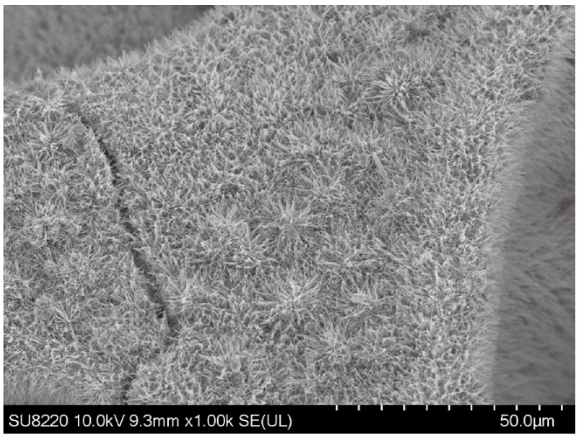

Fig. S3. The morphology of CuO/CF nanowires arrays grown on the copper foam at different magnification.

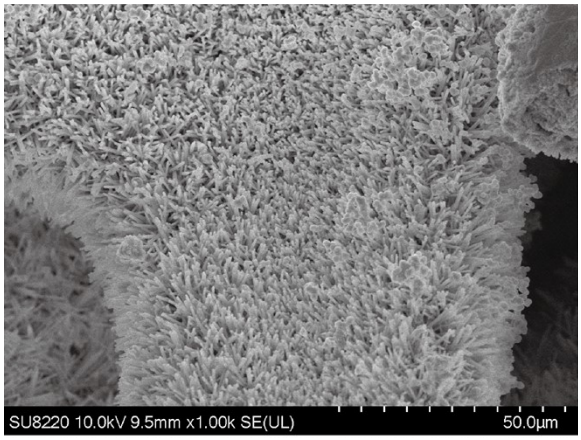

Fig. S4. The morphology of $NiMoO_4$@CuO/CF nanosheets arrays at different magnification.

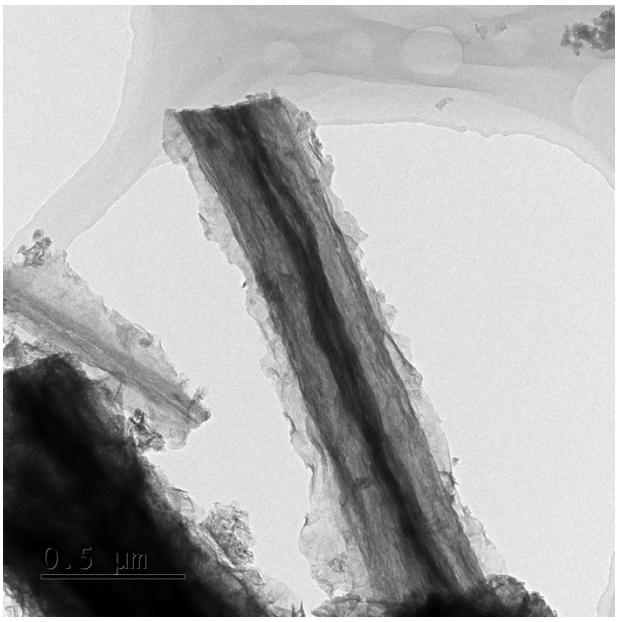

Fig. S5. Typical TEM image of $NiMoO_4$@CuO/CF

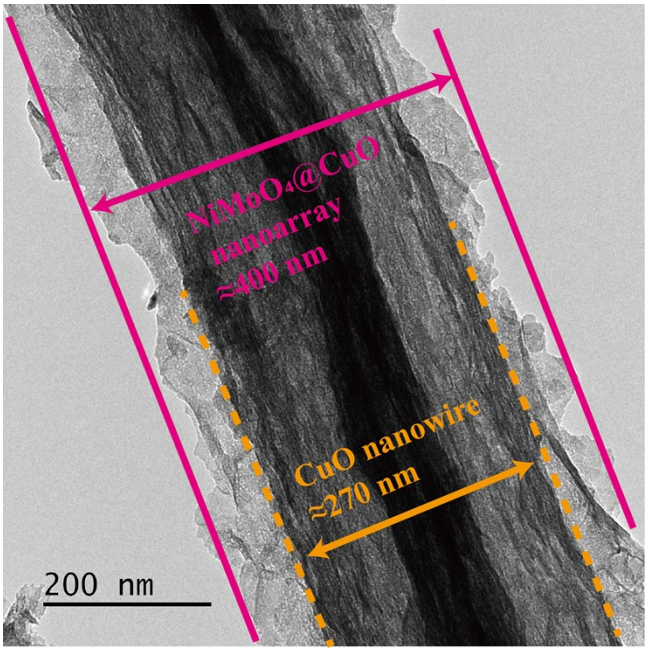

Fig. S6. Typical TEM image of $NiMoO_4$@CuO/CF.

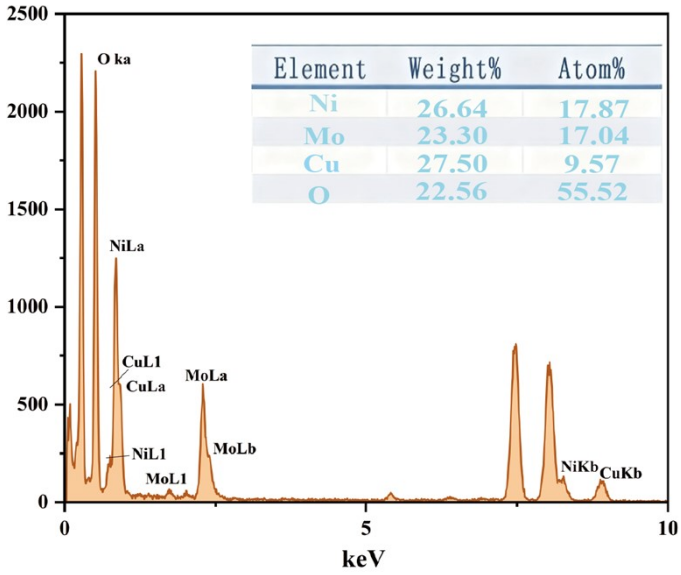

Fig. S7. Elemental distribution and proportions in various regions of $NiMoO_4$@CuO/CF.

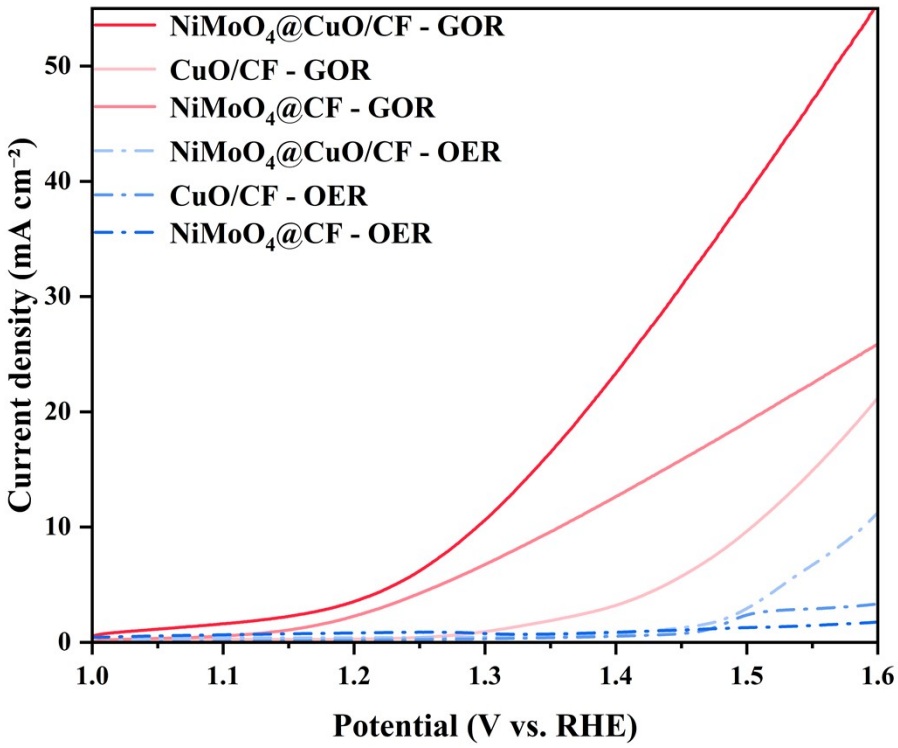

Fig. S8. LSV curves of $NiMoO_4$@CuO/CF, $NiMoO_4$@CF, and CuO/CF in 1 m KOH with and without 0.1 m glycerol addition (without iR-corrected).

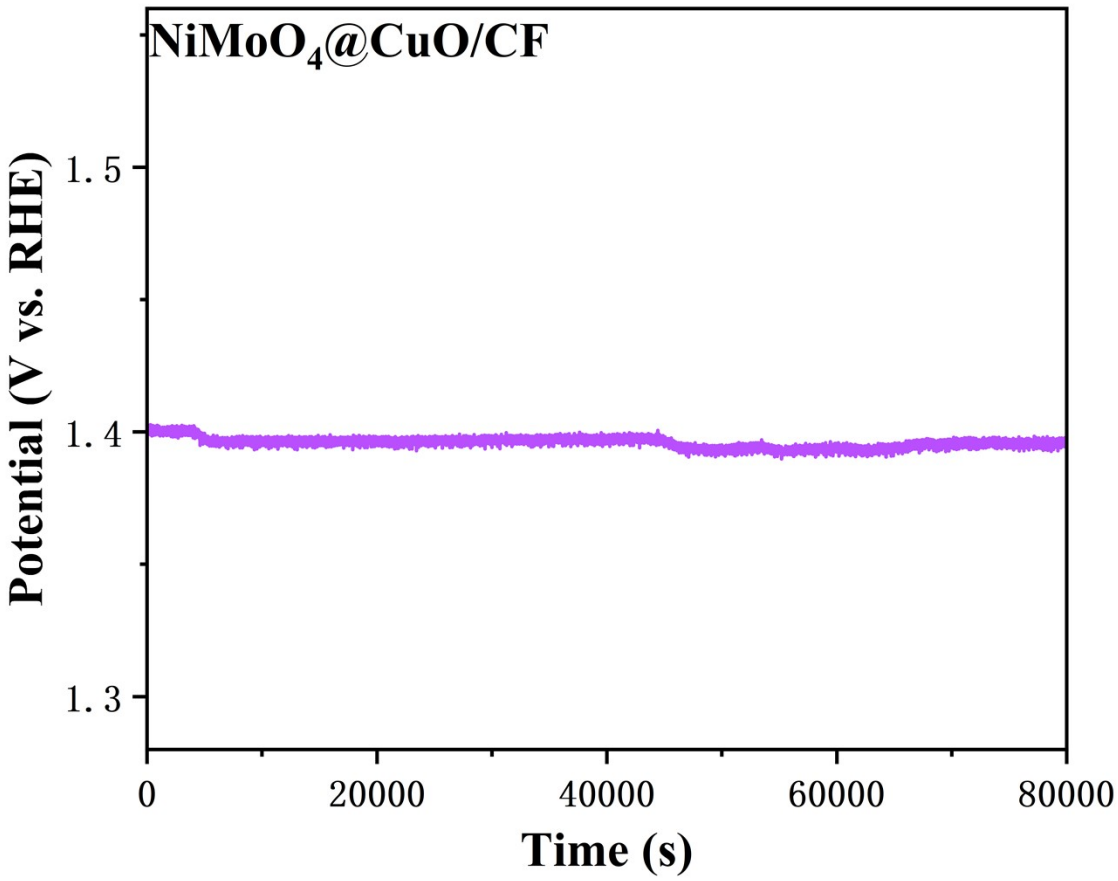

Fig. S9. Long-term electrochemical stability (chronoamperometry) of the $NiMoO_4$@CuO/CF catalyst.

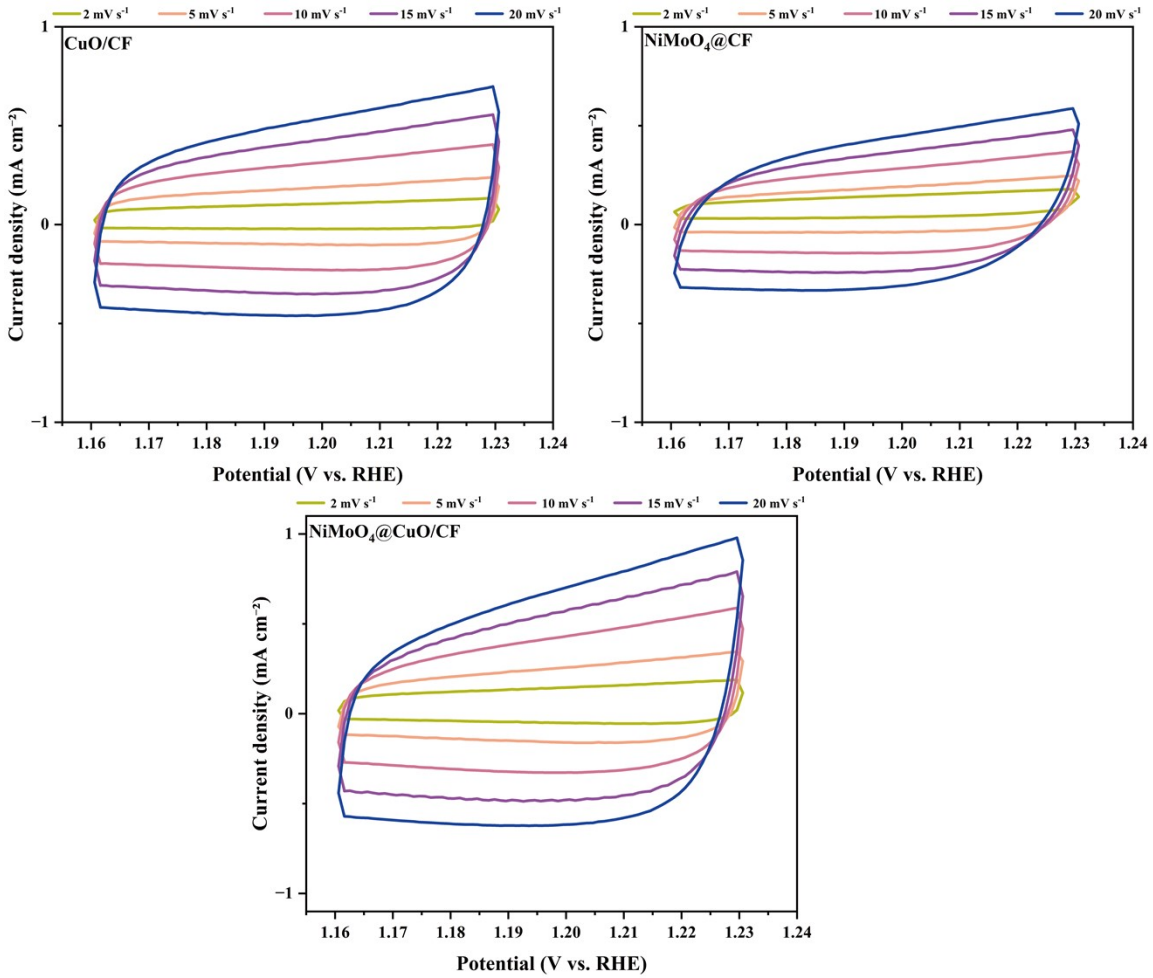

Fig. S10. CV curves of (a) CuO/CF, (b) $NiMoO_4$@CF and (c) $NiMoO_4$@CuO/CF, in the non-faradaic regions at different scan rates.

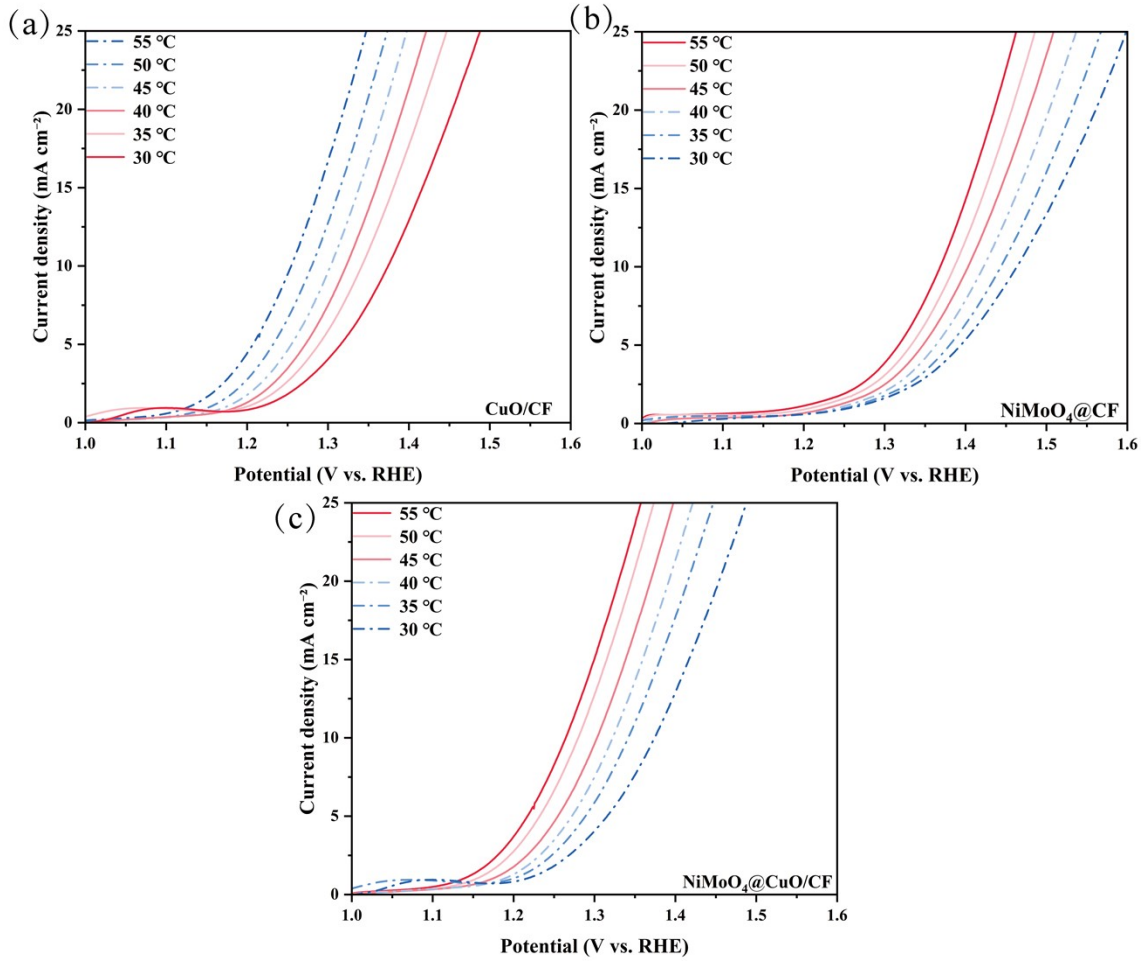

Fig. S11. Glycerol electrocatalytic oxidation performance of the catalysts. LSV curves of a) CuO/CF,) $NiMoO_4$@CF, c) $NiMoO_4$@CuO/CF, in 1 m KOH with 0.1 M glycerol addition (with iR-corrected).

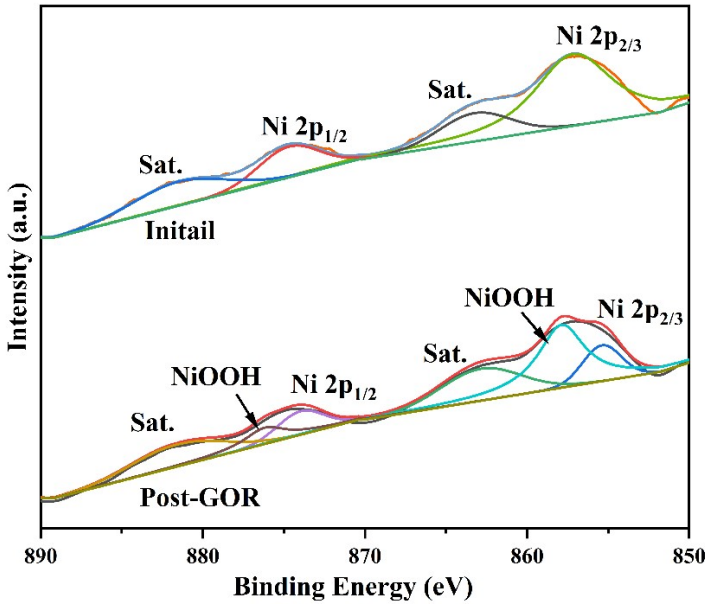

Fig. S12. The high resolution XPS of Ni 2p before (up) and after (down) 100 h GOR test.

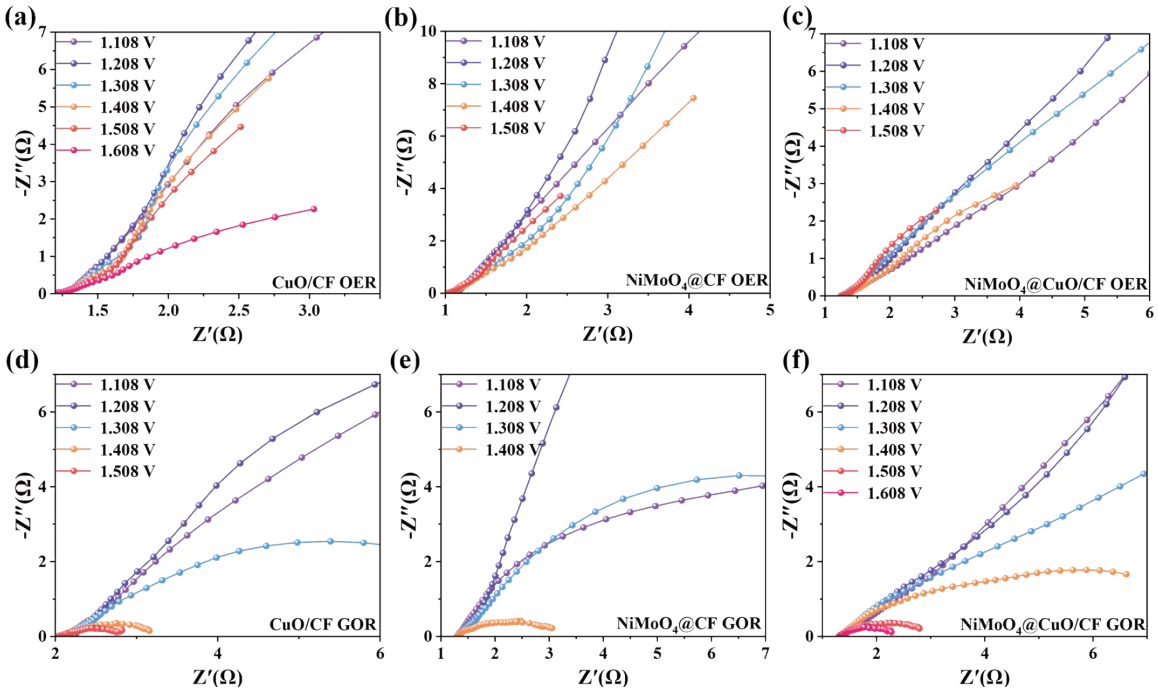

Fig. S13. Nyquist plots of CuO/CF, NiMoO4@CFand NiMoO4@CuO/CF in (a, b, c) 1.0 M KOH and (d, e, f) 1.0 M KOH + 0.1 M glycerol.

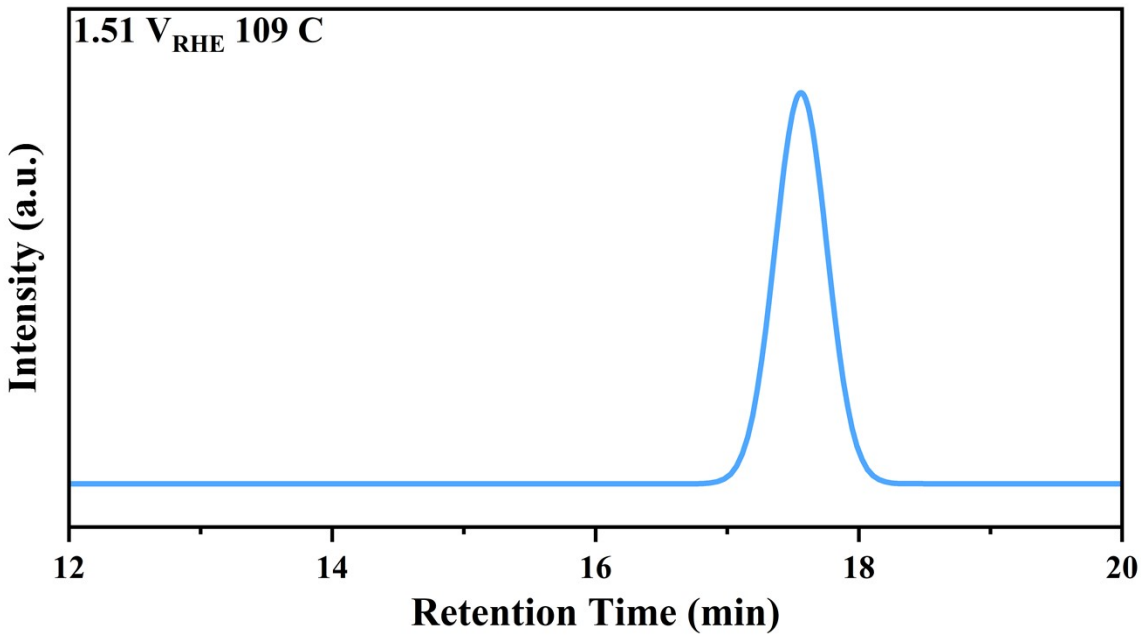

Fig. S14. Enlarged HPLC elution curve of electrolyte at 109C of GOR.

Table S1. The comparison of 'GOR to FA' performance between $NiMoO_4$@CuO/CF and the state-of-the-art catalysts.

Catalysts	Tafel Slope (mV/dec)	Conditions	Con. (%)	FA Sel. (%)	FE.of FA (%)	Ref.
$NiMoO_4$@CuO/CF	96.6	1.51 V_{RHE}; 0.1 M GLY; 1 M KOH.	~100	84.3	90.3	This work.
S-CuO/CF	108	1.35 V_{RHE}; 0.1 M GLY; 1 M KOH.	-30	95.1	95.7	1
$Ni(OH)_2$/NF	/	1.50 V_{RHE}: 0.1 M GLY; 2 M KOH.	/	/	81.3	2
Mn-$CoSe_2$/CFC	157.1	1.27V_{RHE}: 0.1 M GLY; I M KOH.	/	/	-95	3

SA-Bi/Co_3O_4	76.5	1.35 V_{RHE}; 0.1 M GLY; 1 M KOH.	~20	97	97	4
$NiCo_2O_4$/NF	73	1.40 V_{RHE}: 0.1 M GLY; I M KOH.	-20	93.7	89.9	5
NiCo Hydroxide	68.8	1.62 V_{RHE}: 0.1 M GLY; I M KOH.	-89	84	94.3	6
NiVRu-LDHs/NF	102.7	1.40 V_{RHE}: 0.1 M GLY; 1 M KOH.	/	/	-97	7
Ru-NiP/N-C/NF	86.0	1.45V_{RHE}; 0.1 M GLY; 1 M KOH.	~90	-80	93	8
CoCuMaMoNi High Entropy Alloy	53.5	1.32 V_{RHE}: 0.1 M GLY; I M KOH.	/	/	-93	9
Cu-CuS/BM	/	1.45V_{RHE}; 0.1 MGLY;0.1 M KOH.	-40	86.0	90.4	10
$ZnFe_xCo_{2-x}O_4$	163.0	1.62V_{RHE}; 0.5 M GLY; 1 M KOH.	-36	69.5	-50	11
$NiCo(OH)_2$@HOS/NF	35.0	1.35 V_{RHE}; 0.1 M GLY; I M KOH.	-90	81.8	~74	12
Ni_xB	/	1.80V_{RHE}: 0.1 M GLY; I M KOH	73.0	80.0	/	13

References

1. R. Y. Fan, X. J. Zhai, W. Z. Qiao, Y. S. Zhang, N. Yu, N. Xu, Q. X. Lv, Y. M. Chaiand B. Dong, Nano-Micro Lett., 2023, 15, 190.

2. J. X. Wu, J. L. Li, Y. F. Li, X. Y. Ma, W. Y. Zhang, Y. M. Hao, W. B. Cai, Z. P. Liuand M. Gong, Angew. Chem. Int. Ed., 2022, 61, e202113362.
3. L. F. Fan, Y. X. Ji, G. X. Wang, Z. F. Zhang, L. C. Yi, K. Chen, X. Liu and Z. H. Wen, J. Energy Chem., 2022, 72, 424-431.
4. Y. Wang, Y. Q. Zhu, Z. H. Xie, S. M. Xu, M. Xu, Z. Z. Li, L. N. Ma, R. X. Ge, H. Zhou, Z. H. Li, X. G. Kong, L. R. Zheng, J. H. Zhou and H. H. Duan, ACS Catal., 2022, 12, 12432-42433.
5. W. S. Luo, H. Tian, Q. Li, G. Meng, Z. W. Chang, C. Chen, R. X. Shen, X. Yu, L. B. Zhu, F. T. Kong, X. Z. Cui and J. L. Shi, Adv. Funct. Mater., 2023, 2306995.
6. Z. Y. He, J. W. Hwang, Z. H. Gong, M. Z. Zhou, N. Zhang, X. W. Kang, J. W. Han and Y. Chen, Nat. Commun., 2022, 13, 3777.
7. Q. Z. Qian, X. Y. He, Z. Y. Li, Y. X. Chen, Y. F. Feng, M. Y. Cheng, H. K. Zhang, W. T. Wang, C. Xiao, G. Q. Zhang and Y. Xie, Adv. Mater., 2023, 35, 2300935.
8. Y. Xu, T. T. Liu, K. K. Shi, H. J. Yu, K. Deng, X. Wang, Z. Q. Wang, L. Wang and H. J. Wang, J. Mater. Chem. A., 2022, 10, 20365-20374.
9. L. F. Fan, Y. X. Ji, G. X. Wang, J. X. Chen, K. Chen, X. Liu and Z. H. Wen, J. Am. Chem. Soc., 2022, 144, 7224-7235.
10. J. W. Du, Y. Qin, T. Dou, J. M. Ge, Y. P. Wang, X. H. Zhao, F. Z. Zhang and X. D. Lei, ACS. Appl. Nano Mater., 2022, 5, 10174-10182.
11. H. B. Wan, C. C. Dai, L. J. Jin, S. Z. Luo, F. X. Meng, G. Chen, Y. Duan, C. T. Liu, Q. F. Xu, J. M. Lu and Z. C. Xu, ACS. Appl. Mater. Interfaces, 2022, 14, 1429314301.
12. Y. H. Pei, Z. F. Pi, H. Zhong, J. Cheng and F. M. Jin, J. Mater. Chem. A., 2022, 10, 1309-1319.
13. S. Cychy, S. Lechler, Z. J. Huang, M. Braun, A. C. Brix, P. Blumler, C. Andronescu, F. Schmid, W. Schuhmann and M. Muhler, Chin. J. Catal., 2021, 42, 2206-2215.